

The galactic unclassified B[e] star HD 50138[★]

I. A possible new shell phase

M. Borges Fernandes¹, M. Kraus², O. Chesneau¹, A. Domiciano de Souza³, F. X. de Araújo^{★★4}, P. Stee¹, and A. Meilland⁵

¹ UMR 6525 H. Fizeau, Univ. Nice Sophia Antipolis, CNRS, Observatoire de la Côte d'Azur, Av. Copernic, 06130 Grasse, France
e-mail: marcelo.borges@obs-azur.fr, olivier.chesneau@obs-azur.fr, philippe.stee@obs-azur.fr

² Astronomický ústav, Akademie věd České republiky, Fričova 298, 251 65 Ondřejov, Czech Republic
e-mail: kraus@sunstel.asu.cas.cz

³ UMR 6525 H. Fizeau, Univ. Nice Sophia Antipolis, CNRS, Observatoire de la Côte d'Azur, Parc Valrose, 06108 Nice, France
e-mail: armando.domiciano@unice.fr

⁴ Observatório Nacional, Rua General José Cristino 77, 20921-400 São Cristóvão, Rio de Janeiro, Brazil
e-mail: araujo@on.br

⁵ Max-Planck-Institut für Radioastronomie, Auf dem Hügel 69, 53121 Bonn, Germany
e-mail: meilland@mpi-fr-bonn.mpg.de

Received; accepted

ABSTRACT

Context. The observed spectral variation of HD 50138 has led different authors to classify it in a very wide range of spectral types and luminosity classes (from B5 to A0 and III to Ia) and at different evolutionary stages as either HAeBe star or classical Be.

Aims. Based on new high-resolution optical spectroscopic data from 1999 and 2007 associated to a photometric analysis, the aim of this work is to provide a deep spectroscopic description and a new set of parameters for this unclassified southern B[e] star and its interstellar extinction.

Methods. From our high-resolution optical spectroscopic data separated by 8 years, we perform a detailed spectral description, presenting the variations seen and discussing their possible origin. We derive the interstellar extinction to HD 50138 by taking the influences of the circumstellar matter in the form of dust and an ionized disk into account. Based on photometric data from the literature and the new Hipparcos distance, we obtain a revised set of parameters for HD 50138.

Results. Because of the spectral changes, we tentatively suggest that a new shell phase could have taken place prior to our observations in 2007. We find a color excess value of $E(B-V) = 0.08$ mag, and from the photometric analysis, we suggest that HD 50138 is a B6-7 III-V star. A discussion of the different evolutionary scenarios is also provided.

Key words. Stars: fundamental parameters – Stars: winds, outflows – Stars: individual: HD 50138

1. Introduction

Stars that present the B[e] phenomenon are known to form a heterogeneous group. This group is composed of objects at different evolutionary stages, such as high- and low-mass evolved stars, intermediate-mass pre-main sequence stars, and symbiotic objects (Lamers et al. 1998). However, for more than 50% of the confirmed galactic B[e] stars, the evolutionary stage is still unknown, so that they are gathered in the group of the unclassified B[e] stars. This problem is mainly caused by poor knowledge of their physical parameters, especially their distances.

In this paper, we present our study related to the southern B[e] star HD 50138 (V743 Mon, MWC158, IRAS 06491-0654). The spectrum of this star was discussed for the first time by Merrill et al. (1925). Later, the presence of spectral variability

was cited by Merrill (1931) and Merrill & Burwell (1933). Since then, numerous papers have mainly considered this star as either a pre-main sequence star, more specifically as a Herbig Ae/Be star, or as a classical Be star. Jaschek et al. (1993) have even considered this star as a transition object between a classical Be and a B[e] star. Later Lamers et al. (1998) and Zorec (1998) include this star in the list of unclassified B[e] stars.

The difficulty in obtaining the correct classification of HD 50138 is mainly caused by the strong spectral variability as reported in the literature. Pogodin (1997) cites the presence of different scales of spectral variability, from days to months, especially in the line profiles of $H\alpha$, HeI (λ 5876), and Nar lines. Spectral variations have also been identified in the UV, by the analysis of IUE spectra (Hutsemékers 1985). These spectral variabilities have been explained by an outburst that possibly happened in 1978-1979 (Hutsemékers 1985) and by a shell phase in 1990-1991 (Andrillat & Houziaux 1991). On the other hand, HD 50138 had presented small and non-periodic photometric variations that did not seem to be associated to the spectral changes related to this shell phase (Halbedel 1991).

In addition, studies based on polarimetry and spectropolarimetry have identified an intrinsic polarization that seems

* Based on observations (i) with the 1.52-m and 2.2-m telescopes at the European Southern Observatory (La Silla, Chile), under agreement with the Observatório Nacional-MCT (Brazil), and (ii) with the Telescope Bernard Lyot, Observatory of Pic du Midi (France).

** It is with great sadness that we have to report that, during the final stages of this paper, we had a deep loss when Francisco X. de Araújo passed away.

to be linked to nonspherical symmetry of matter around this object, probably a circumstellar disk (Vaidya et al. 1994; Bjorkman et al. 1998; Oudmaijer & Drew 1999; Harrington & Kuhn 2007). A disk-scattering effect associated to an outflow has also recently been suggested by Harrington & Kuhn (2009).

On the other hand, Cidale et al. (2001) propose that this object could be a binary system. Based on spectro-astrometry, Baines et al. (2006) suggest the same possibility, where the companion would be separated by $0.5'' - 3.0''$. However, up to now, no direct evidence of binarity has been found.

HD 50138 was further observed during the Hipparcos mission, and its distance of 290 ± 71 pc (Perryman et al. 1997) turned out with 500 ± 150 pc to be almost doubled according to the new data reduction procedure performed by van Leeuwen (2007). The newly determined distance and the large uncertainties in the previously published stellar classification attempt request and warrant detailed investigation and revision of the stellar parameters of HD 50138.

In this study, we present our new optical spectroscopic observations and perform a photometric and spectroscopic analysis of HD 50138, aimed on the one hand at describing the observed spectral variations and, on the other, at better constraining the stellar parameters, needed for an improved discussion about the nature of this object.

The paper has the following structure. In Sect. 2 we describe our observations. In Sect. 3, we present our results. In Sect. 3.1, we describe our high-resolution spectra taken on different dates. In Sect. 3.2, we derive from the analysis of our spectroscopic data and public photometric measurements, the interstellar and circumstellar extinction, hence the stellar parameters and the spectral type of this object. In Sect. 4, we discuss the possible scenarios for explaining the nature of this curious star, and finally in Sect. 5, we present our conclusions.

2. Observations

We obtained high-resolution optical spectra using the high-resolution Fiber-fed Extended Range Optical Spectrograph (FEROS) and the Narval spectro-polarimeter. The first FEROS spectrum was obtained on October 27, 1999, when the spectrograph was attached to the 1.52-m telescope, and the second was obtained on October 4, 2007, when it was attached to the 2.2-m telescope, both at the European Southern Observatory in La Silla (Chile). FEROS is a bench-mounted Echelle spectrograph with fibers, which covers a sky area of $2''$ of diameter, with a wavelength coverage from 3600 \AA to 9200 \AA and a spectral resolution of $R = 55\,000$ (in the region around 6000 \AA). We adopted its complete automatic online reduction, where the heliocentric correction is done.

The spectrum of 1999 was obtained with an exposure time of 180 seconds and has S/N of approximately 80 in the 5500 \AA region. In 2007, we were able to take two consecutive spectra of the star, both with 180 seconds of exposure time. Since these spectra do not show significant differences, we added them up for a better S/N, which is around 250.

Concerning the Narval data, they were obtained on March 14, 2007. Narval is an Echelle spectro-polarimeter attached to the telescope Bernard Lyot at the observatory of Pic du Midi (France). For this study, we are only using the spectroscopic data that cover a sky area of $2.8''$ of diameter, with a wavelength range from 3750 \AA to 10500 \AA and a spectral resolution of $R = 80\,000$. We obtained 8 exposures of 300 seconds each. The S/N is around 360. We also adopted its complete automatic online re-

duction; however, due to problems related to the merging of the spectral orders (especially in the region of the Balmer lines), we use this spectrum mainly for a qualitative comparison with the FEROS data, which are of better quality for our purposes.

3. Results

3.1. Spectral description of HD 50138

The high-resolution spectra of HD 50138 present lines from neutral and singly ionized elements. In addition to many emission lines with circumstellar origin, HD 50138 exhibits absorption lines, which are probably formed in the stellar photosphere. Our spectra were taken 8 years apart and strong spectral variations can be noted. Similar variations were previously reported in the literature and associated to shell phases and outburst events (Doazan 1965; Hutsemékers 1985; Andriolat & Houziaux 1991; Bopp 1993; Pogodin 1997).

Table 1 lists all lines present in our FEROS spectra, along with their radial velocities (obtained considering the center of the lines and the laboratory wavelength of each transition), equivalent widths of emission and absorption components, and the possible identification¹. For some lines there are more than one possible classification, however the radial velocity is derived assuming the first identification cited. There, “Uid” means that the line is unidentified. Because of uncertainties in the position of the underlying continuum, we estimate the errors of our measurements to be about 20% for the faint lines and about 10% for the strongest lines. Especially for the faint lines, there is also a significant difference between the radial velocities measured in 1999 and in 2007. This difference probably comes not only from circumstellar changes, but also from the low S/N of our 1999 data. The behavior of the lines from the main elements present in our spectra is described here.

– Hydrogen

In our FEROS spectra, we identify the presence of Balmer lines (see Table 1). Four of them, $H\delta$, $H\gamma$, $H\beta$, and $H\alpha$ can be seen in Fig. 1. The profiles of these lines, except for $H\alpha$, are composed of a broad absorption component, probably of photospheric origin, and an emission and a narrow absorption components superimposed, which are probably formed in the circumstellar medium. This kind of profile was already described by Houziaux (1960) from observations taken in the late fifties. The $H\alpha$ line presents a double-peaked structure, where the V/R changes from 0.36 in 1999 to 0.88 in 2007. These values are different than those found by Halbedel (1991) and Pogodin (1997) of 0.6 and 0.5, respectively. However, the peak separation presents small differences in both our spectra, $\sim 160 \text{ km s}^{-1}$ in 1999 and 150 km s^{-1} in 2007, in agreement with the value cited by Oudmaijer & Drew (1999) of $\sim 160 \text{ km s}^{-1}$.

Another significant variation is related to the radial velocities of the narrow absorption components. In 1999, this value is almost constant for $H\delta$, $H\gamma$, and $H\beta$, $\sim 35 \text{ km s}^{-1}$. However in 2007, this value is quite different for each line, 95 km s^{-1} ($H\delta$), 60 km s^{-1} ($H\gamma$) and 50 km s^{-1} ($H\beta$). The $H\alpha$ line’s central absorption presents a constant value of $\sim 60 \text{ km s}^{-1}$ on both dates. This velocity is quite different from the velocity reported by

¹ In order to identify the lines, we used the line lists provided by Moore (1945), Thackeray (1967), and Landaberry et al. (2001). We also looked up two sites on the web: NIST Atomic Spectra Database Lines Form (URL physics.nist.gov/cgi-bin/AtData/lines_form) and The Atomic Line List v2.04 (URL <http://www.pa.uky.edu/~peter/atomic>).

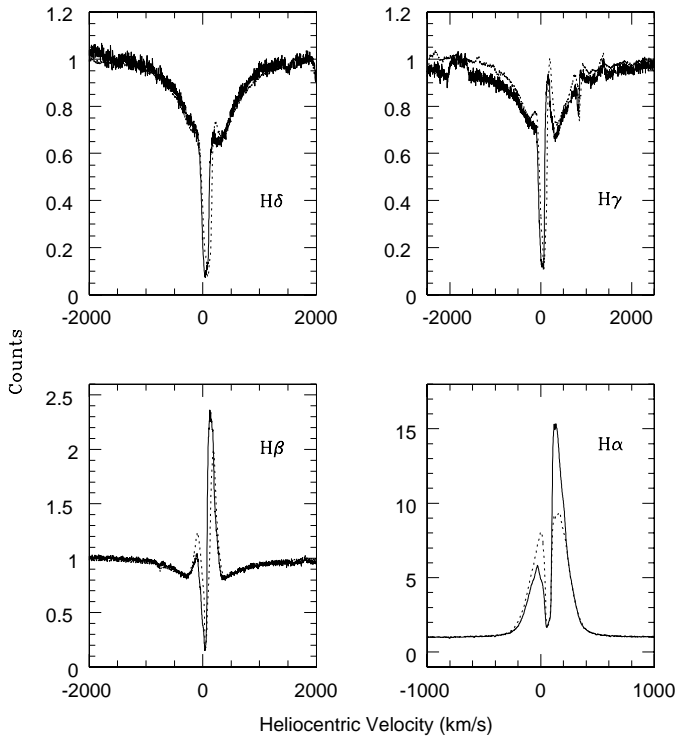


Fig. 1. Balmer lines seen in the FEROS spectra of HD 50138. The solid line is related to the spectrum taken in 1999 and the dotted line to the 2007 one.

Oudmaijer & Drew (1999); however, this can be related to different spectral resolutions. As cited by Pogodin (1997), the Balmer lines also present symmetric wings, which show velocities that can reach $\sim 1500 \text{ km s}^{-1}$, as can be seen in Fig. 1 and even better in the blow-up of the $H\alpha$ wings in Fig. 2. However, these high velocities seem to come from electron scattering, since no other element identified in our data present such characteristic.

We identify Paschen 22 to Paschen 12 lines in our spectra. We show one of these lines, Paschen 19, in Fig. 3. They display strong variations in our FEROS and Narval data. In the 1999 FEROS data, we detect a single-peaked profile with a blue shoulder. This shoulder becomes more prominent, probably because of the better S/N, in the Narval data. However, with the 2007 FEROS data, we clearly have a double-peaked profile with a peak separation of 190 km s^{-1} . Assuming the shoulder previously seen in 1999 and in the Narval data as another peak, we have a variation of V/R in the 2007 FEROS data. A similar variation was reported by Andrillat & Houziaux (1991), which was associated to an outburst. The wings of Paschen lines are extended in all spectra to $\sim 300 \text{ km s}^{-1}$. However, as seen in Table 1, we believe the radial velocities obtained for the Paschen lines are affected by some problems with the precision of the wavelength calibration of FEROS, beyond 8300 \AA .

– Iron

Iron, as can be seen in Table 1, is by far the element with the most of lines identified in our spectra, with all of them from FeII. We have identified permitted and forbidden lines. The latter are represented by narrow single-peaked emission lines from multiplets 3, 4, 6, 7, 17, 18, 19, 20, 21, and 34. These forbidden lines do not present any noticeable difference in all spectra.

We have identified permitted lines from the multiplets 20, 21, 25, 26, 27, 28, 30, 37, 38, 41, 42, 43, 49, 55, 73, 74, 167, 190,

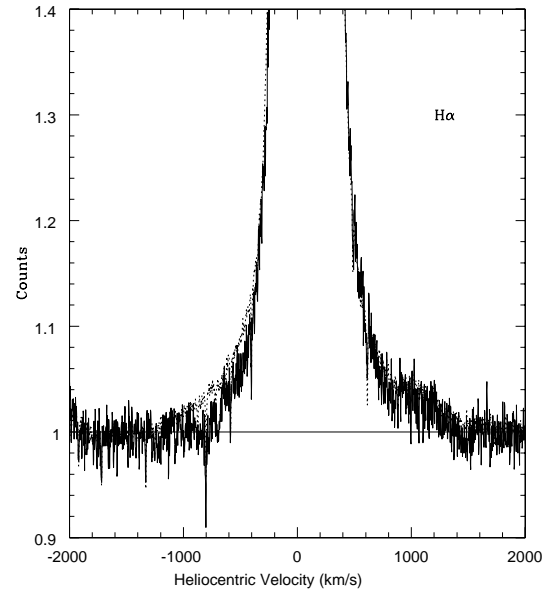


Fig. 2. $H\alpha$ wings seen in the FEROS spectra of HD 50138. The different line styles have the same meaning as in Fig. 1. The normalized continuum is also presented for better visualization.

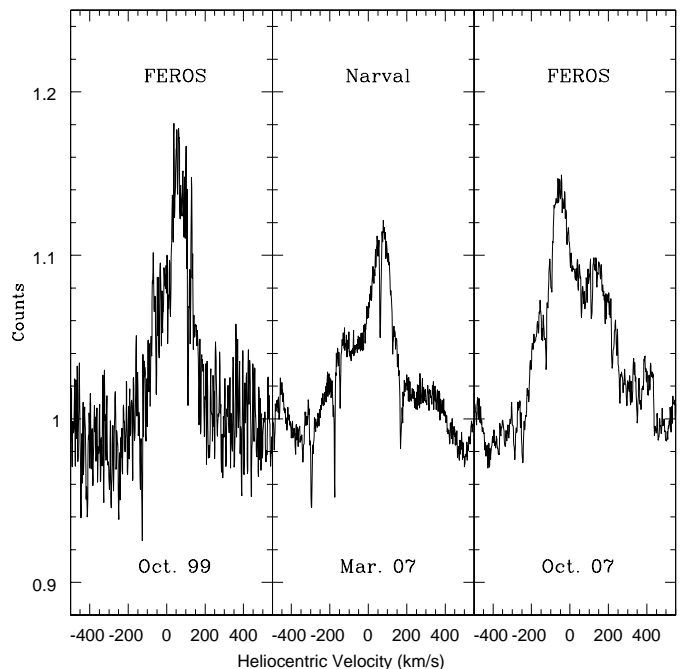


Fig. 3. Variations in the line profile of Paschen 19 at 8413 \AA .

200, and 203. Unlike Jaschek & Andrillat (1998), where the FeII lines show absorption (mainly) or emission profiles, our spectrum presents a special kind of profile for each date (see Fig. 4). In the 1999 FEROS spectrum, these lines have a P-Cygni profile, where the absorption component is made up of two components, with the bluer one being more intense. In the 2007 FEROS spectrum, these lines have a different profile. There is an emission profile associated to a strong central absorption that also has two components, where the bluer one is also more intense. These absorption components are shifted to higher velocities compared

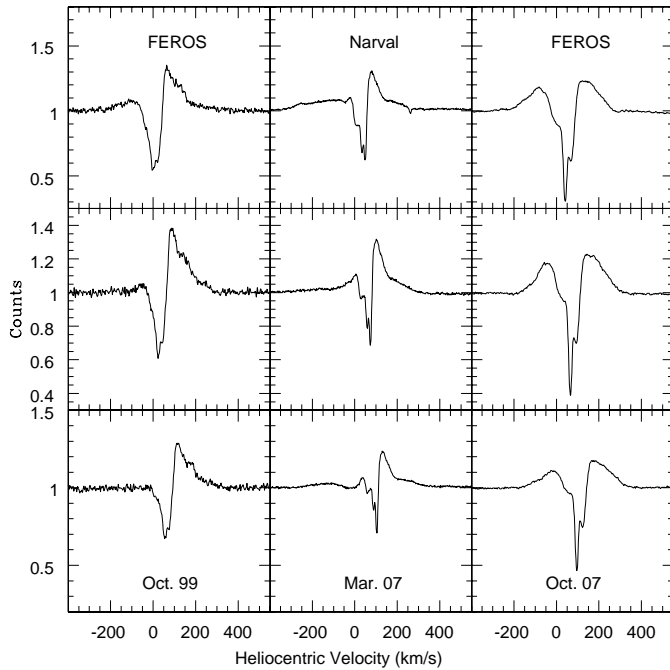


Fig. 4. Variations in the line profiles of the FeII multiplet 42. The bottom line corresponds to the line at 4923Å, the middle one to 5018Å, and the top one at 5169Å.

to 1999. On the other hand, the Narval data show a sort of transition between the P-Cygni profile and the profile seen in the 2007 FEROS spectrum. The absorption components are not as intense as seen in the other spectra; however, three of them can be seen, where the red one, contrary to the FEROS data, is the most intense.

– Oxygen

Permitted and forbidden lines of neutral oxygen are seen in the HD 50138 spectra. No OII lines were identified, indicating that the emission region is not highly ionized or that the higher ionized regions are rather small in volume, suppressing the efficient production of observable OII emission and absorption. The forbidden lines present narrow emission profiles and do not show any significant differences in all the spectra, with an almost constant radial velocity around 40 km s⁻¹ (Table 1). All three lines from the multiplet 1 are seen, different than reported by Andrillat & Houziaux (1972). In addition, a contamination by airglows, based on the comparison with spectra from the sky taken at the same time, is discarded.

The permitted lines present a complex profile and show a strong variation in the different spectra (see Fig. 5). The line centered at 7774Å is in fact a triplet, thus the profile seen in our data has a combination of possible emission and absorption components from each line. However, the profile of this triplet changes strongly at different dates, as already mentioned by Jaschek & Andrillat (1998). Unlike the 1999 data, the 2007 FEROS data show the absorption components clearly superimposed over a strong emission component, similar to the FeII lines. In the Narval spectrum, this line has a transitional profile between those detected in the different FEROS spectra, especially in the emission component.

Another oxygen line present in our spectra is located at 8446Å. This line presents a strong emission in the FEROS spectrum of 1999 and in the Narval data; however, this profile

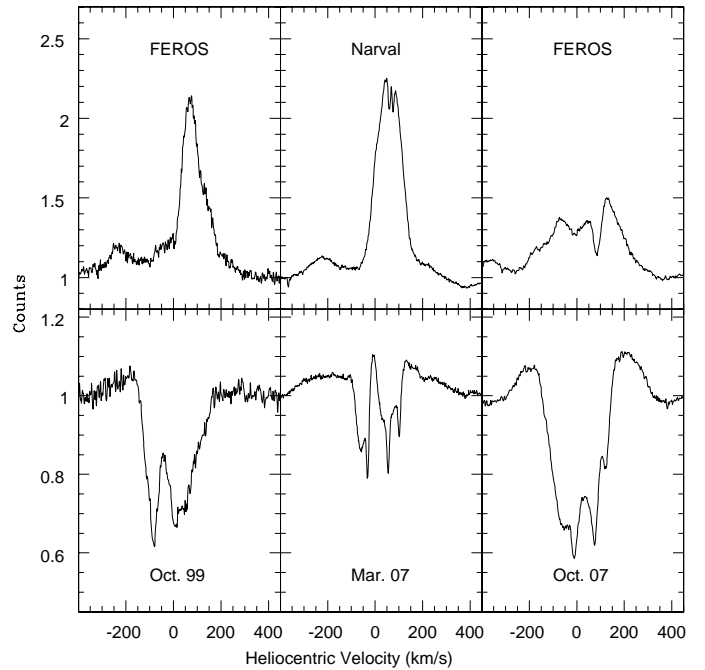


Fig. 5. Profiles of the permitted lines of OI and their variation. The bottom line corresponds to the triplet at 7774Å and the top one at 8446Å.

changes completely in the FEROS spectrum of 2007, because it is less intense and has multiple peaks.

– Helium

HD 50138 presents several HeI lines from multiplets 2, 10, 11, 12, 14, 16, 18, 20, 22, 46, 47, 51, 53, and 55. Line profile variations are clearly seen in the different spectra (Fig. 6). In 1999, we can see an inverse P-Cygni profile for some lines, such as 5876Å. The separation seen between the emission and the absorption components agrees with the value cited by Bopp (1993), ~ 200 km s⁻¹. However, in 2007, profiles similar as seen for the FeII lines are formed, where the absorption component is narrower than in 1999. Both profiles present wings with similar extension velocities, as can be seen in Fig. 6. Similar variations were described by Bopp (1993), who reported an inverse P-Cygni profile, a few months after the outburst in 1991, and also by Pogodin (1997), who cited that the profile of the line at 5876Å, changes from night to night.

Our spectra do not show any HeII line. The tentative detection of the HeII line at 10123Å, as reported by Jaschek & Andrillat (1998), could not be confirmed by our Narval data. We can therefore claim that this object is not very hot.

– Magnesium

Only one line from MgI, at 6318Å, is identified in our spectra. On the other hand, few lines from MgII are seen in our data, with the most prominent one, at 4481Å. This line mainly has photospheric origin, and as can be seen in Fig. 7, it also presents a noticeable variation in our FEROS data taken with 8 years of difference.

– Silicon

In the FEROS spectrum of 1999, SiII lines have pure absorption profiles. On the other hand, in March 2007, the lines of the

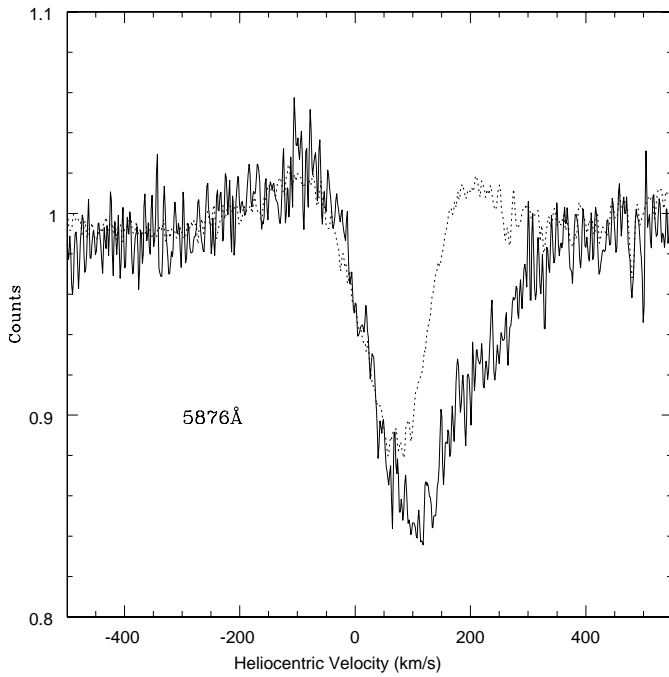


Fig. 6. Line profile variation of the He I line at 5876 Å. The solid line is related to the spectrum taken in 1999 and the dotted line to the 2007 one.

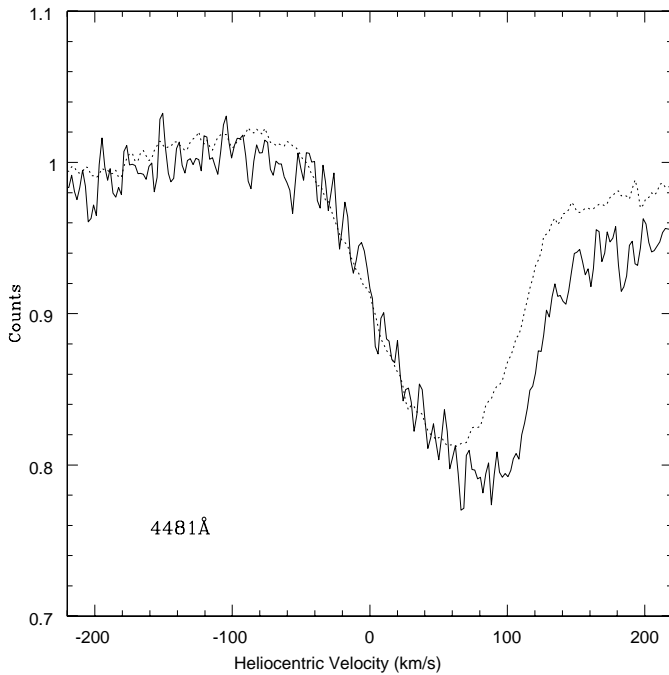


Fig. 7. As in Fig. 6 but for the Mg II line at 4481 Å.

multiplet 2 ($\lambda\lambda$ 6347,6371) developed into an inverse P-Cygni profile, which is even more pronounced in October 2007, as can be seen in Fig. 8 for one of these lines. However, the lines of the multiplet 3 ($\lambda\lambda$ 4128,4131) still show pure absorption profiles at these dates (see Fig. 9) and might thus be considered as having a pure photospheric origin.

– Sodium

Lines of Na I are present in our spectra at 5890 Å and 5895 Å. These lines are formed by a combination of circumstellar and

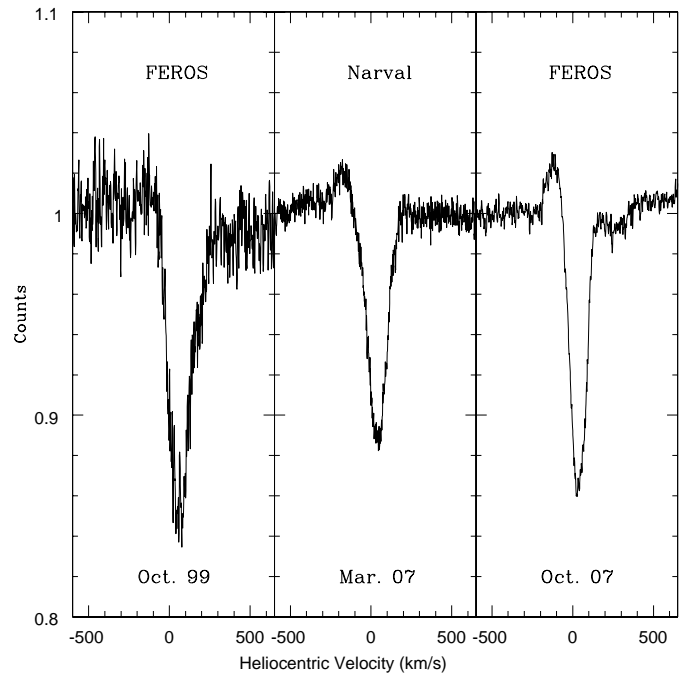


Fig. 8. The variation of the line profile of Si II at 6347 Å.

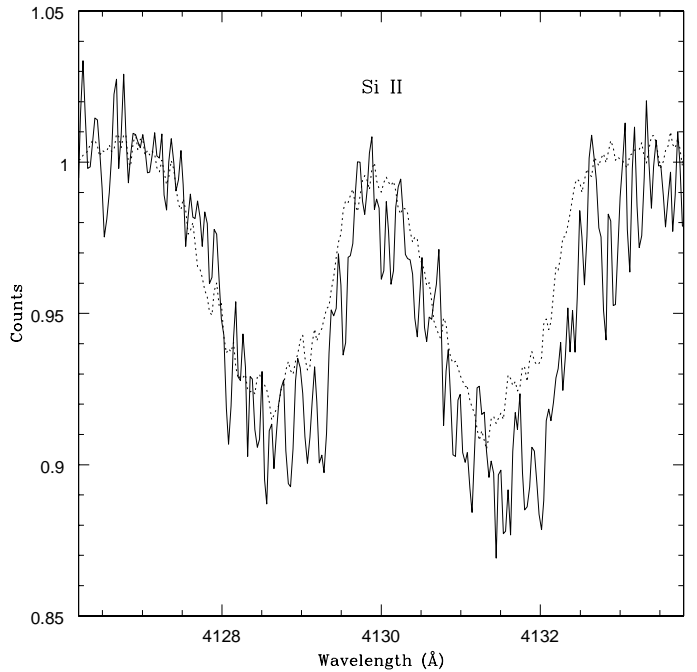


Fig. 9. As in Fig. 6 but for the Si II lines at 4128 Å and 4131 Å.

interstellar contributions. However, it is impossible for us to disentangle each component, which makes it impossible to derive a distance to HD 50138 from these lines. These lines also present variability from 1999 to 2007 (Fig. 10), because it is almost a P-Cygni profile, with three absorption components in 1999 and a broad emission component superimposed by three absorption components in 2007.

– Other lines

Permitted lines from Ti II, Ca II, Cr II, Cu II, Si II, and Ni I are also identified in our spectra (see Table 1). These lines also show sig-

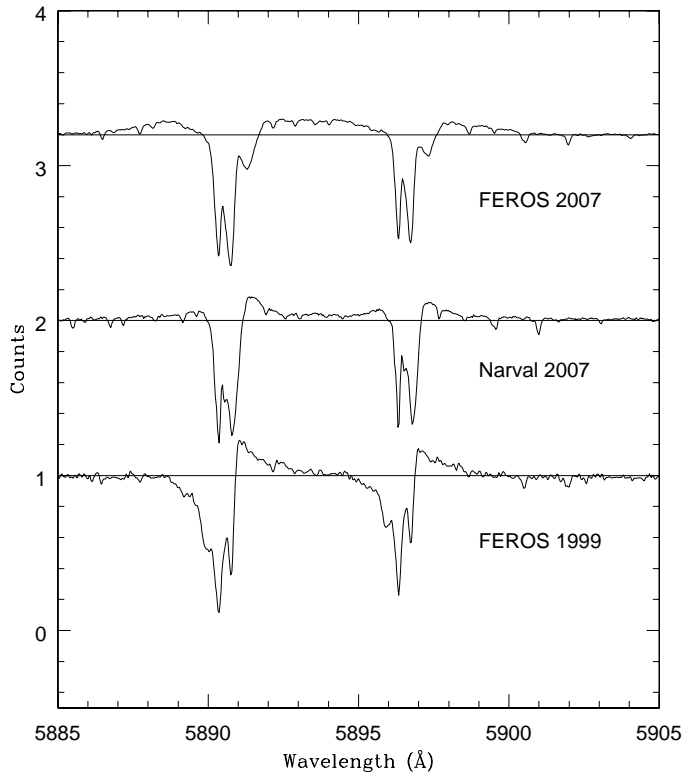


Fig. 10. Different line profiles of the NaI lines at 5890Å and 5896Å. The normalized continuum is also presented for each date.

nificant differences from 1999 to 2007, following the same behavior as described for the FeII lines.

3.2. Determination of the extinction and spectral classification

The determination of the stellar parameters of HD 50138 is difficult, since both its spectral lines and its continuum show strong variations. It is, therefore, not surprising that the range of spectral types (from earlier than B5 down to A0) and luminosity classes (I-V) found in the literature is rather wide, because we can expect that these determinations depend on the method (or lines) used for the classification, as well as on the period at which the observations were obtained.

To constrain the spectral classification of HD 50138, we made use of both our own sets of high-resolution optical spectra and public photometric data. We collected all available *UBVRI* band photometric data. These observations cover a time interval of almost 25 years and are displayed in Fig. 11. The references for the data are listed in Table 2.

Unfortunately, hardly any photometric data could be found before and around the time of the outburst, which was reported to have happened in 1978/79 (Hutsemékers 1985). The consequences of this outburst are, however, clearly visible in the light curves displayed in Fig. 11: a fading of the star in the *UBV* bands by about 0.2 mag, and a recovery to the old brightness after about 5 years. This trend in photometric data might be explained by some large mass ejection during the outburst, hiding the stellar continuum inside a dense shell or ring of (partly) optically thick material, which then turns transparent during expansion, allowing the underlying star to be seen again. On the other hand, the shell phase seen in the optical spectra in 1990/91 (Andrillat

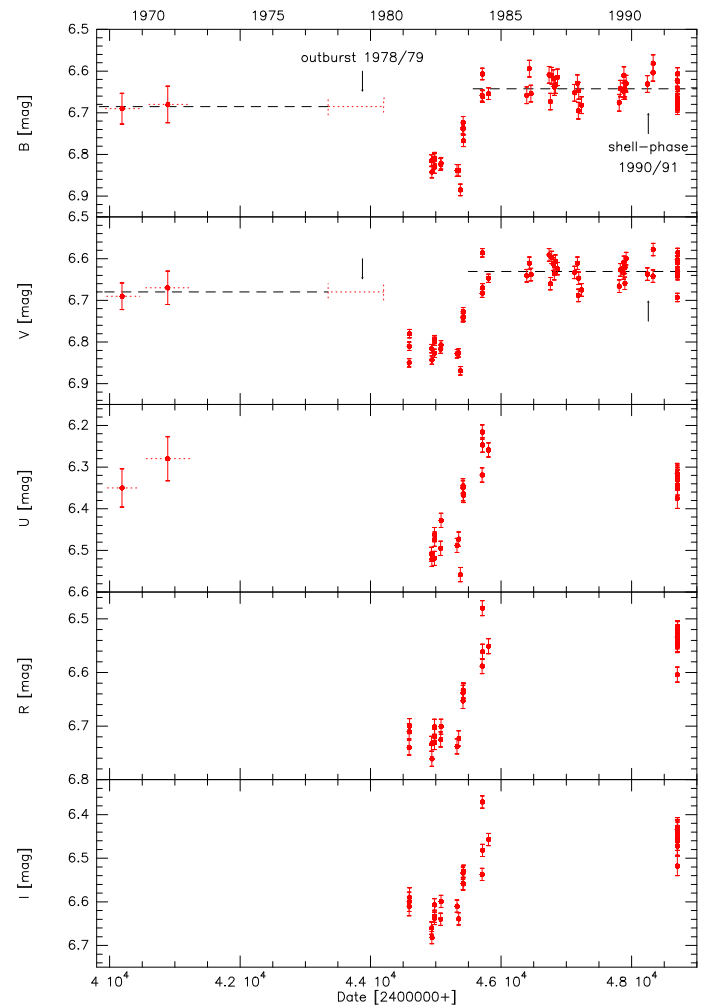


Fig. 11. Time variation of photometric observations in the *UBVRI* bands collected from the literature (see Table 2). Also shown are the supposed positions of the outburst and the shell phase reported in the literature. The dashed lines in the *B* and *V* bands indicate the mean values before and after the outburst. The dotted bar in the *B* and *V* light-curves refer to the observations of Alvarez & Schuster (1981).

Table 2. References to the *UBVRI* observations of HD 50138 shown in Fig. 11.

Julian Dates [2400000+]	Reference
39916 – 40464	Haupt & Schroll (1974)
40556 – 41224	Penston (1973)
43350 – 44200	Alvarez & Schuster (1981)
44589 – 44596	de Winter et al. (2001)
44934 – 45809	Kilkenny et al. (1985)
46392 – 48331	Halbedel (1991)
48699 – 48707	de Winter et al. (2001)

& Houziaux 1991) remained invisible in the photometric data, as cited by Halbedel (1991). This might indicate that the shell phase was caused by mass ejection with much less mass loss.

Interestingly, after the recovery of the star, it seems to be even brighter than it was before the outburst, as can be seen by

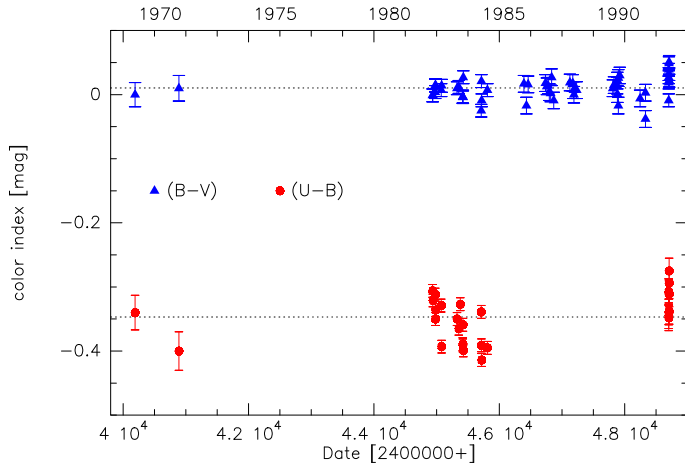


Fig. 12. Time variation of the observed $(U - B)$ and $(B - V)$ color indices.

the comparison of the mean values before and after the outburst (Fig. 11). We also notice that the mean value before is based only on two datapoints, but even considering the large errorbars of these observations, it seems that the star appears brighter after ~ 1984 . In addition, Alvarez & Schuster (1981) observed HD 50138 in a period close to the outburst, but without providing either the exact dates or the observed magnitudes. However, these authors claimed that during their observations, HD 50138 was not variable, compared to previous observations, meaning that ΔB and $\Delta V < 0.02$ mag, according to their definition of variability.

This apparent brightening after ~ 1984 might be caused by some contribution of the circumstellar material ejected during the outburst and after adding flux at all bands. Even though HD 50138 is known to possess a strong infrared excess emission due to circumstellar dust (Allen 1973), this dust will hardly contribute at optical wavelengths, i.e., in the UBV bands. On the other hand, based on spectropolarimetric observations performed in 1995 by Bjorkman et al. (1998), HD 50138 seems to have an almost edge-on ionized Be-like disk. Such a disk, which might have been formed from the outburst material in a similar way to how disks are formed around classical Be stars, can well add flux to the optical continuum in the form of free-free and especially free-bound emission.

Whether the additional continuum emission from the ionized circumstellar material/disk will hamper proper spectral classification of HD 50138, or whether we even have to account for circumstellar dust along the line of sight towards the star, acting as a further (i.e. circumstellar) extinction source, will be discussed and investigated in detail in Sects. 3.2.3 and 3.2.2, respectively.

3.2.1. The interstellar extinction

First, we estimate the total extinction towards HD 50138, i.e., neglect any circumstellar contribution and thus derive an upper limit on the interstellar one. For this, we make use of the two color indices $(U - B)$ and $(B - V)$. Their variations with time are plotted in Fig. 12.

Obviously, $(U - B)$ is quite variable, while $(B - V)$ remains rather stable, even during the outburst phase. Despite the variability in $(U - B)$, we can obtain a reasonable range for the possible stellar classification from these observed color indices, making use of the following relations for the interstellar extinction

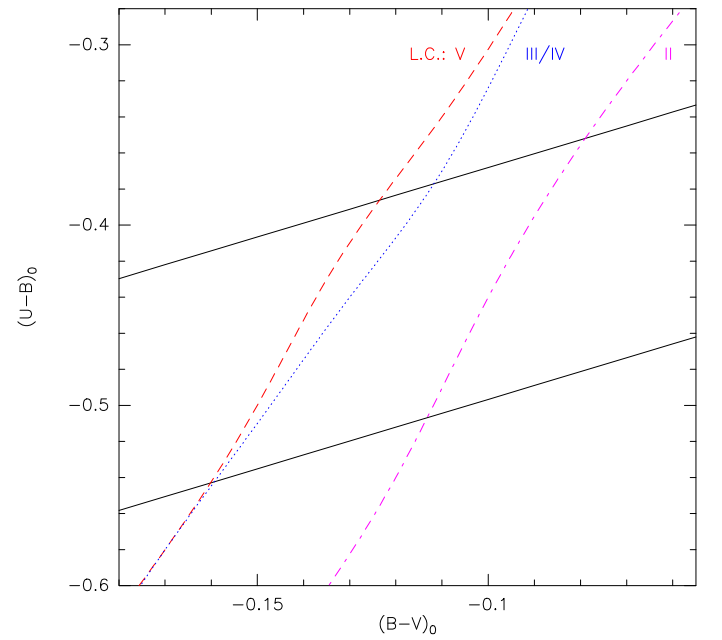


Fig. 13. Constraining the range in spectral type for different luminosity classes. The solid lines correspond to the upper and lower limits derived from observations.

determinations,

$$E(B - V) = (B - V) - (B - V)_0 \quad (1)$$

$$E(B - V) = \frac{1}{0.77} E(U - B) = \frac{1}{0.77} \{ (U - B) - (U - B)_0 \}. \quad (2)$$

The second relation follows from Leitherer & Wolf (1984), and the parameters $(U - B)_0$ and $(B - V)_0$ refer to the intrinsic color indices. By combining these two equations, we obtain for each observed set of $(U - B)$ and $(B - V)$ colors a reddening independent equation of the form

$$(U - B)_0 = 0.77 \{ (B - V)_0 - x \}, \quad (3)$$

relating the two intrinsic colors, with

$$x = (B - V) - \frac{(U - B)}{0.77}. \quad (4)$$

We calculate the parameter x , hence the relation Eq. (3), for each observation. Then we search for the two boundary cases, i.e., the highest and lowest values for x , and plot the resulting range in relation Eq. (3) in Fig. 13. Next, we look up the tables of Schmidt-Kaler (1982) for the intrinsic colors of stars in the spectral range B3 to A1. The luminosity class of HD 50138 is not well known, but previous classifications found in the literature tend towards luminosity classes III-V (e.g., Houziaux 1960; Houziaux & Andrillat 1976; Frémat et al. 2006). Based on the Hipparcos distance, we can already exclude a supergiant classification for HD 50138, since it would deliver an unrealistically high extinction value. We thus restrict it to luminosity classes II to V.

The behavior of the intrinsic colors from Schmidt-Kaler (1982) is included in Fig. 13. From the overlap with the observational ranges we find some preliminary sets, as listed in Table 3, of MK types, effective temperatures and color excess values, which are upper limits to the real interstellar extinction. The assignment of the temperature ranges is made based on the tables of Flower (1996).

Table 3. Possible stellar classifications of HD 50138 under the assumption of pure interstellar extinction along the line of sight.

L.C.	Sp.Type	$T_{\text{eff}}[K]$	$E(B-V)_{\text{max}}[mag]$
V	B5.5–7.5	$13\,300 \pm 900$	0.15 ± 0.03
III/IV	B5.5–8.0	$13\,100 \pm 1\,100$	0.15 ± 0.03
II	B7.5–8.5	$11\,600 \pm 400$	0.11 ± 0.02

A rather low value for the interstellar extinction has already been suggested by Houziaux & Andriolat (1976) and Hutsemékers (1985) based on the weakness of the interstellar feature at $\lambda 2175 \text{ \AA}$ and on the absence of interstellar lines in the IUE spectrum. To split the total extinction value into its interstellar and (possible) circumstellar contributions we, therefore, search for further extinction indicators in our spectra. One such indicator makes use of diffuse interstellar bands (DIBs). In our high-resolution spectra, we found one reasonably good DIB at $\lambda 5780 \text{ \AA}$, from which the extinction can be derived (see Herbig 1993). This feature is present in both the 1999 and the 2007 FEROS spectra, but because of the poor S/N of the 1999 data we can rely only on our 2007 data. From the equivalent width of 0.04 \AA of this DIB, we derive an extinction value of $E(B-V) = 0.08 \pm 0.01 \text{ mag}$.

As a further check we investigate the interstellar extinction within the galactic plane in the region around our target. It turns out that HD 50138 is located within a region of rather low extinction (see Neckel & Klare 1980; Chen et al. 1989; Arenou et al. 1992). Using the model developed by Hakkila et al. (1997) for the large-scale visual interstellar extinction, assuming $R_V = A_V/E(B-V) = 3.1$, we have obtained $A_V = 0.22 \pm 0.22 \text{ mag}$, delivering $E(B-V) = 0.07 \pm 0.07 \text{ mag}$. This value agrees with the value we found from the DIB. However, because of higher uncertainty (and definitely larger error) with this method, the value found from the DIB of $E(B-V) = 0.08 \pm 0.01 \text{ mag}$ seems to be reasonably accurate, leading us to use this value later. Compared to the (upper limit) values we found from the color indices, the contribution of the interstellar extinction towards HD 50138 is thus only half of it, indicating that the other part must be circumstellar in nature.

3.2.2. The influence of circumstellar dust

The presence of a strong infrared excess implies that HD 50138 must be surrounded by circumstellar dust (Allen 1973). How this dust is distributed, i.e., whether it is situated within a disk or shell, within or outside the line of sight, is not known.

The circumstellar dust, like the interstellar one, absorbs and scatters the light from the star, so that we can define a circumstellar extinction parameter, A_{UBV}^{dust} . The intrinsic magnitude of the star in each photometric band, UBV_0 , is then obtained from the observed one, corrected for the amounts of interstellar and circumstellar extinction, i.e.,

$$UBV_0 = UBV_{\text{obs}} - \left(\frac{A_{UBV}}{A_V} \right)_{\text{ISM}} A_V^{\text{ISM}} - A_{UBV}^{\text{dust}}, \quad (5)$$

with the parameters $(A_{UBV}/A_V)_{\text{ISM}}$ resulting from the mean interstellar extinction curve (see e.g. Cardelli et al. 1989; Mathis 1990). A star that suffers from additional circumstellar extinction thus appears fainter.

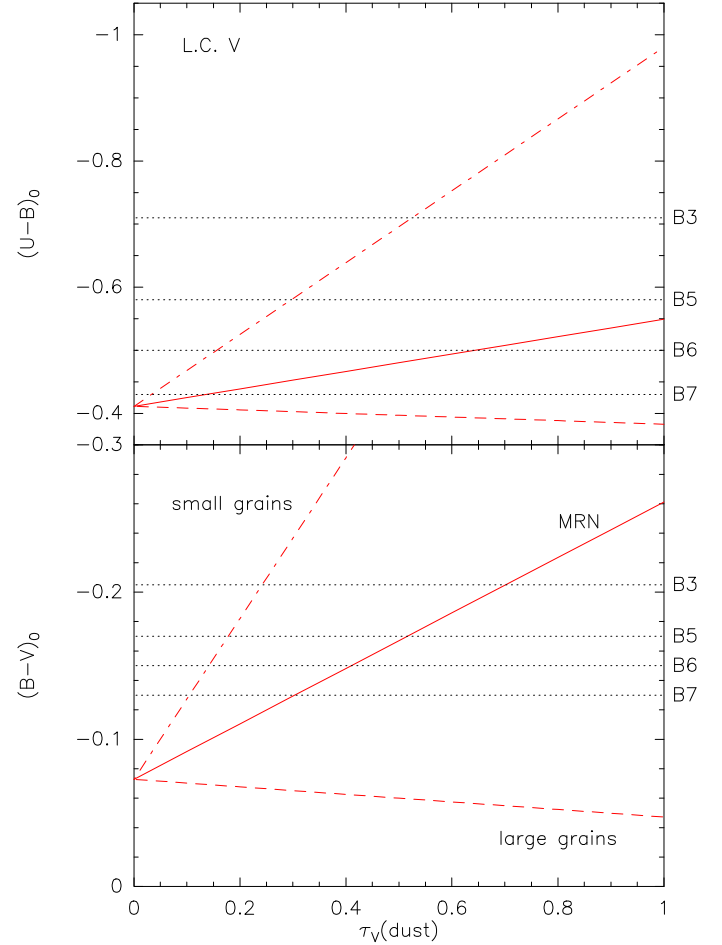


Fig. 14. Intrinsic colors as a function of dust optical depth. Individual curves represent calculations performed for a mixture of silicates and amorphous carbon grains for either single (smallest and largest, as cited in the text) grain sizes or an MRN grain size distribution. The dotted lines indicate theoretically expected intrinsic colors for different spectral types.

The dust extinction parameter, A_{UBV}^{dust} , can be calculated from

$$A_{UBV}^{\text{dust}} = \frac{1}{0.4 \ln(10)} \frac{\sigma_{UBV}^{\text{ext}}}{\sigma_V^{\text{ext}}} \tau_V^{\text{dust}}, \quad (6)$$

with σ^{ext} as the extinction coefficient of the dust within the corresponding band and τ_V^{dust} as the optical depth of the dust at visual wavelengths. The extinction coefficients depend on the size of the grains and their chemical composition. Since the dust composition along the line of sight is not known, we allow for different sizes of the (spherically) test grains, which we consider as composed either of amorphous carbon or silicates. The range of sizes used extends from $7.5 \times 10^{-3} \mu\text{m}$ up to $\sim 1 \mu\text{m}$. In addition to single grains of different sizes, we consider the well-known MRN grain size distribution (Mathis et al. 1977).

For each grain size and species, the dust extinction depends on only one free parameter, which is τ_V^{dust} . Expressing the set of Eqs. (5) by the intrinsic color indices $(U-B)_0$ and $(B-V)_0$, we end up with two equations

$$(U-B)_0 = f(\tau_V^{\text{dust}}), \quad (7)$$

$$(B-V)_0 = f(\tau_V^{\text{dust}}). \quad (8)$$

These calculated intrinsic colors for different dust optical depths can then be compared to theoretically expected color indices of stars with different spectral type and luminosity class (e.g. Schmidt-Kaler 1982), in order to constrain the range of possible spectral classifications.

The results are shown in Fig. 14 for stars with luminosity class V, but the results for the other luminosity classes are very similar. Plotted are the dependences of the two intrinsic color indices on τ_V^{dust} computed for the smallest and largest grains, as well as for the MRN grain size distribution, using a mixture of silicates and amorphous carbon. The theoretically expected values for the different spectral types are also shown. Obviously, an agreement between the computed and theoretical color indices (delivering the same dust optical depth) is achieved only for stars with spectral type between B6 and B7. Very similar results are found for the luminosity classes III/IV, while for stars with luminosity class II we find a possible spectral range of B8-8.5.

Interestingly, pure large grains are not able to account for the circumstellar extinction. Instead, the circumstellar dust along the line of sight must consist of predominantly small grains, which can be located in an optically thin dust sphere or shell, in agreement with the results of Bjorkman et al. (1998). However, other scenarios, like a dusty disk where the dust is not in our line of sight or is optically thin, since it is formed far from the star, cannot be discarded. An interferometric analysis will probably answer this question about the circumstellar dust geometry (Borges Fernandes et al., in preparation).

3.2.3. The influence of the ionized circumstellar disk

The contribution of an ionized envelope or disk to the total continuum emission of early-type stars was the subject of many detailed investigations during the past years. For the case of classical Be stars, for instance, Zorec & Briot (1991) found a relation between the excess emission in the *V* band (defined as the difference between the *V* band magnitudes measured during the Be phase and the non-Be phase) and the effective temperature of the star. Their relation indicates a stronger circumstellar contribution for hotter (i.e., earlier) Be stars, while late-type Be stars hardly show any contamination of their *V* band fluxes by their circumstellar ionized material. A similar trend was found by detailed numerical studies of Stee & Bittar (2001), who found circumstellar contributions to the continuum in the *B* and *V* bands for a B5e star of 0.57% and 6.01%, respectively, while the contributions are found to be much lower for later types. But not only are classical Be stars influenced by their ionized circumstellar material, B-type supergiants can also have a significant wind contribution at all optical bands, as recently shown by Kraus et al. (2008; 2009).

B[e] stars are generally believed to have disks with higher densities than classical Be stars. In this case, an influence of the free-free and at optical wavelengths, especially of the free-bound continuum emission, might thus be expected. But in contrast to circumstellar dust, which acts at optical wavelengths as a pure absorber that dims the stellar light, the free-free and free-bound processes act not only as an absorber, but at the same time as an additional emission component, which adds more flux at a given wavelength than it absorbs from the underlying stellar flux. A star with an ionized disk thus usually appears brighter at all wavelengths compared to a star with no ionized disk (see Kraus et al. 2008; 2009).

We check the influence of such an ionized circumstellar disk on the proper spectral type determination by calculating the emission of free-free and free-bound processes in circumstellar

disks of different densities. The shape of the continuum emission of the ionized gas does not severely depend on the geometry of the ionized material. For instance, a spherically symmetric wind and a geometrically flat disk result in the same shape of the wavelength dependent free-free and free-bound continuum emission. This indicates that the identical continuum flux distribution can be obtained from quite different geometrical scenarios. In addition, the free-free and free-bound continuum at optical wavelengths is generated in the close vicinity of the star, typically within $2 - 5 R_*$ (Kraus et al. 2008). It can thus not offer any insight into the global disk density distribution and geometry.

Since our aim is only to obtain proper stellar parameters, but not a global description of the detailed geometry and density variations within the highly dynamical and non-spherically symmetric circumstellar material, for which we definitely have too little observational information at hand, we study the influence of the ionized disk emission on the color indices in a very simplified way.

From the literature values (see Fig. 11) we computed the pre-outburst average observed magnitudes in the *UBV* bands, deredden them with the interstellar extinction value derived in Sect. 3.2.1, and convert them into fluxes. These fluxes correspond to the star plus disk system. Then, individual disk fluxes in the *UBV* bands were calculated. For this, we adopted a very simple disk model whose surface density distribution can be described by

$$\Sigma(r) = \Sigma_0 * \frac{R_*}{r}. \quad (9)$$

Such a surface density distribution follows, e.g., for the case of an outflowing disk forming wind, which might be an appropriate model. In that case, the surface density at the inner edge of the disk is given by (see Borges Fernandes et al. 2007)

$$\Sigma_0 = \frac{\dot{M}\alpha}{4\pi R_* v} \quad (10)$$

where \dot{M} describes the (here constant) mass loss rate over the disk-forming wind region, α is the disk opening angle, and v the disk outflow velocity.

The disk fluxes (in the form of free-free and free-bound emission) in the *UBV* bands, resulting from disks with increasing values of Σ_0 , are then subtracted from the observed and interstellar extinction corrected ones. The resulting pure stellar fluxes are converted back into magnitudes and the color indices are derived. The results are shown in Fig. 15. Obviously, for low surface densities, the contribution of the disk is negligible, while its importance drastically increases with increasing surface density (top panel of Fig. 15).

Because of the increasing disk flux in all three bands with respect to the stellar flux, the star must be intrinsically fainter in all three bands (see Fig. 15), especially influencing the (B-V) color index (lower panel) more than the (U-B) (middle panel). From a comparison of the derived color indices to the expected intrinsic colors of Schmidt-Kaler (1982) for stars of luminosity class V and different spectral types, we find a rather narrow range of valid stellar classifications, as indicated by the box extending over the complete plot in Fig. 15. While for luminosity classes III-V the range in spectral type is B6-7, we find a spectral type of B8 for luminosity class II. These ranges are in fairly good agreement with those found previously. This is not surprising, because the amount of circumstellar extinction is rather small, so that no big changes in intrinsic colors can be expected.

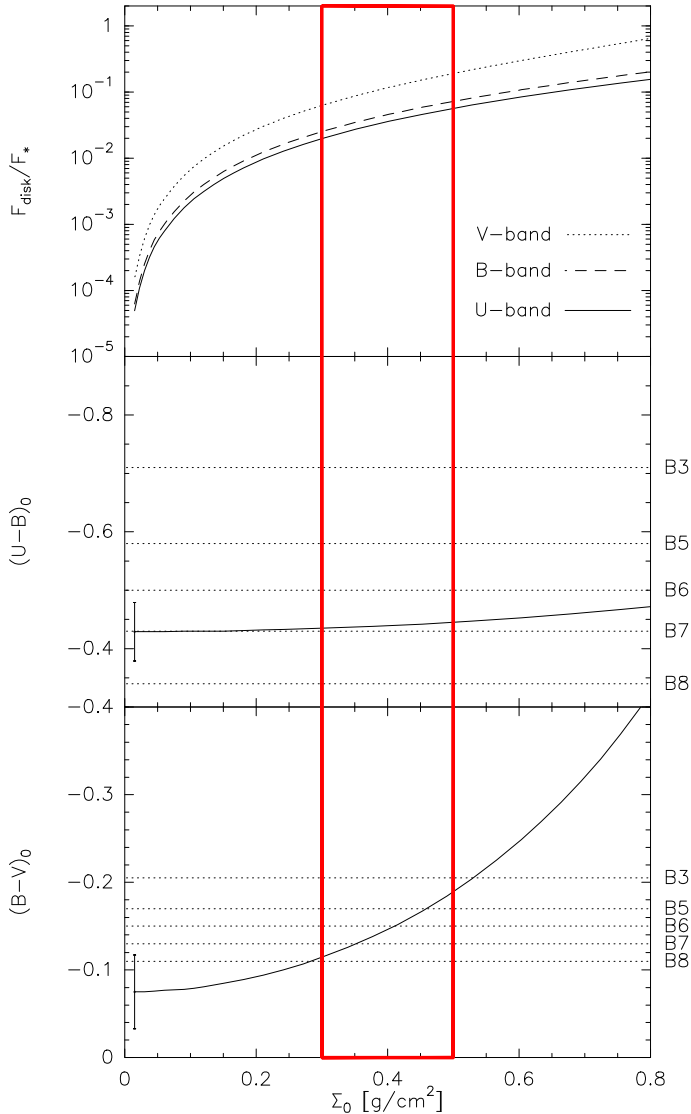


Fig. 15. Increase in disk flux with respect to the stellar flux (top panel) and intrinsic colors (mid and bottom panel) with disk surface density. The dotted lines indicate theoretically expected intrinsic colors for different spectral types and a luminosity class V. The box extending over all three panels gives the range in possible classifications and the corresponding needed disk flux in all three bands.

We would like to emphasize that the surface density chosen for the x -axis to plot our results in Fig. 15 is not the most relevant parameter. Instead, the influence of the disk as shown in the top panel is the crucial parameter here. Such fractions of the free-free and free-bound continuum can also be achieved with quite different geometrical models and density distributions. Nevertheless, the range in values for Σ_0 found from our analysis can easily be achieved with typical values for B[e] stars, e.g., disk opening angles in the range of 5 - 30 degrees, disk outflow velocities of 10 - 100 km s⁻¹, and mass loss rates typically of 10⁻⁸ to 10⁻⁵ M_\odot yr⁻¹. However, the exact value for each parameter cannot be provided by our research due to the lack of reliable information concerning the geometry and dynamics of such a possible pre-outburst ionized disk, and the modeling provided here cannot be regarded as the only valid answer. It was only used to qualitatively discuss the influence of the ionized

material to the color indices of the star in order to constrain the spectral classification of HD 50138. How the ionized material is really distributed around the star cannot be derived from a pure free-free and free-bound emission calculation.

From our analysis of the circumstellar extinction contributions of either the dust or the ionized disk, we find possible classifications of HD 50138 as either a B6-7 III-V star with $T_{\text{eff}} = 13200 \pm 500$ K, or a B8-8.5 II star with $T_{\text{eff}} = 11300 \pm 300$ K. As a further check of these derived classifications, we derived the ratio of the equivalent widths of the most plausible photospheric Si II lines in our spectra. The ratios of the 4131 Å/4128 Å and the 5056 Å/5041 Å equivalent widths are sensitive to temperature and surface gravity and have been computed from the line identification tables obtained with the code SYNSPEC (see Hubeny & Lanz 2000) based on Kurucz (1979) model atmospheres in local thermodynamical equilibrium and Kurucz (1993) line lists. At temperatures between 10 000 K and 12 000 K and surface gravities according to luminosity class II, these ratios show a mild increase with temperature from 1.7 to 1.8 (4131 Å/4128 Å) and from 2.1 to 2.3 (5056 Å/5041 Å), while the observed values, based on Table 1, are 1.41 ± 0.19 and 1.82 ± 0.26 in 1999 and 1.08 ± 0.15 and 1.50 ± 0.21 in 2007. From this discrepancy between observed and calculated equivalent width ratios, a B8-8.5 II scenario for HD 50138 can be excluded. For higher temperatures and especially higher surface gravities, the variations in the equivalent width ratios are no longer strictly correlated, but an overlap in the theoretical and observational values for stars of spectral types in the range B6-7 III-V occurs, so that these equivalent width ratios can be used at least as a qualitative check for consistency. From the photometric results and the qualitative agreement with the equivalent width ratios of Si II lines, we can claim that the final spectral classification of HD 50138 is a B6-7 III-V star. It is important to cite that our results agree with the classification obtained by Zorec et al. (1998) and Cidale et al. (2001) using the BCD (Barbier-Chalonge-Divan) spectrophotometric system, based on the study of the Balmer discontinuity.

To finish our stellar parameter study, we want to determine the possible ranges in stellar luminosities. Our ionized disk model implies a pure stellar V band flux from 6.49 mag to 6.71 mag for the lowest and highest possible disk contributions of 7% and 20%, respectively, in the range of possible MK types. We thus conclude that the star has an intrinsic V band flux of 6.60 ± 0.11 mag. This result has been obtained from considering the pre-outburst photometry only. We also tried it with the post-outburst data. Thanks to the high variability of the data, the results still agree with a B6-7 star but have a higher uncertainty. Using the bolometric corrections for B6-7 III-V stars from Flower (1996) and the Hipparcos distances towards HD 50138 of 500 ± 150 pc, we can finally calculate the stellar luminosity to $\log(L_*/L_\odot) = 3.06 \pm 0.27$.

We did not attempt to derive the luminosities for the case of the circumstellar dust extinction, because (i) based on the observed ionized disk around HD 50138, this possibility seems to be the more realistic one, and (ii) we currently have no clear indication of the possible dust composition and grain size distribution at hand. Nevertheless, assuming the range in dust optical depths obtained by our analysis for the MRN grain size distribution (see Fig. 14), the range of stellar luminosities corrected by the circumstellar dust extinction is in a fairly good agreement with the above derived luminosity range.

4. Discussion of the nature of HD 50138

The variability in the line profiles, as cited by Pogodin (1997), seems to be caused by shell phases and/or outburst events. As described in the Sect. 3.1, from comparison of our spectroscopic data, we saw that there is a sort of temporal evolution, in particular an increase of a blue emission component and a redshift of the absorption ones. Based on this, we believe that a new ejection of material took place prior to our Narval observations, i.e., before March 2007 with increasing emission later on (our second FEROS observation). This new shell phase would be the responsible for the changes seen in our data.

Another possibility is that the material was ejected in our direction, possibly by a hot spot on the stellar surface, forming a kind of “one-armed spiral”, as suggested for classical Be stars. If this was the case, this would mainly explain the blue-shifted emission. On the other hand, even without having complete knowledge of the wind contribution for all lines, we suggested that for some of them, there is no contamination from the wind and they have a pure photospheric origin. Based on this, an extended and expanding atmosphere or a new ring or envelope with a lower outflow velocity that started to expand some time in early 2007 (or slightly earlier) could explain the changes in the radial velocities seen in the photospheric lines (see Fig. 9 and Table 1).

The results of Bjorkman et al. (1998), claiming the existence of intrinsic polarization due to electron scattering, indicate a non-spherically symmetric structure with a gaseous disk seen almost edge-on, in association with an optically thin dust envelope. Our results described in Sect. 3.2.2 confirm that such a scenario for the circumstellar dust is possible.

Based on the stellar parameters derived in Sect. 3.2.3, we can indicate the position of HD 50138 on the HR diagram and compare it to evolutionary tracks. This is shown in Fig. 16, where we plot the evolutionary tracks from Schaller et al. (1992) in the top panel for stars at solar metallicity. From this plot, HD 50138 is a $(5.0 \pm 0.5) M_{\odot}$ star, since still on, or just evolving off, the main sequence. The lower panel of Fig. 16 shows its position compared to pre-main sequence evolutionary tracks from Bernasconi & Maeder (1996). The ZAMS, as well as the birthline are also included. This plot indicates a stellar mass of roughly $(6.0 \pm 1.0) M_{\odot}$, but for a star that is approaching the main sequence.

From the position in the HR diagram alone, it is not possible to distinguish between a pre-main sequence and a post-main sequence evolutionary phase, however we can discuss some points about the possible nature of HD 50138.

- Pre-main sequence nature:

The luminosity and the mass derived by our analysis agree with those expected for an intermediate mass pre-main sequence star. HD 50138 shows similar spectral and photometric variations as seen in young objects. However, if it is a young star close to the main sequence, associated to its high temperature, its maternal cloud would already be dispersed and the remaining dust would be located in the accretion disk. This would be confirmed by the forbidden lines seen in our spectra, which are not blueshifted, as seen in young deeply embedded stars (Waters & Waelkens 1998; Hamann 1994). In addition, based on its rather high temperature, HD 50138 would be a Herbig B[e] star.

On the other hand, the absence of any nebulosity around HD 50138 and its situation far from any star-forming region (Pogodin 1997) is against a Herbig B[e] classification. The possible shell ejection phases are also against a young nature. In

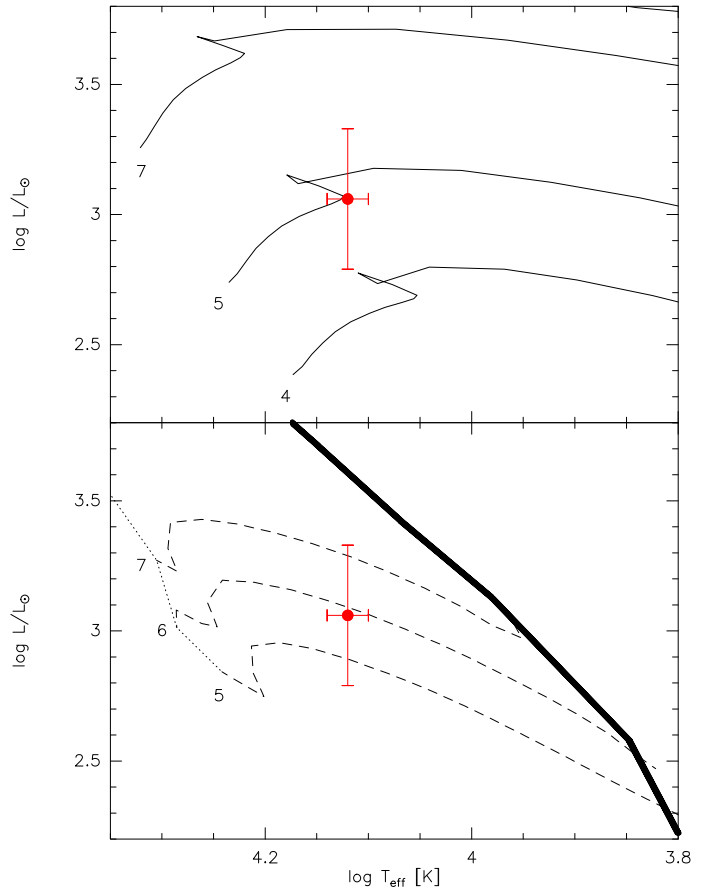


Fig. 16. Position of HD 50138 on the HR diagram compared to post-main sequence (top panel) and pre-main sequence (bottom panel) evolutionary tracks. In the bottom panel, the dotted line defines the zero-age main sequence, the thick solid line defines the birthline.

addition, the results of Bjorkman et al. (1998) show that the dust is probably distributed in an optically thin envelope and not in an accretion disk.

- A Be star close to (or just at the turn-off from) the main sequence:

The classification as a Be star that is still on, or just at the turn-off from, the main sequence cannot be ruled out at this moment. However, two points are against the classification of HD 50138 as a classical Be star: the forbidden lines and the IR excess due to dust. The formation of dust in an intermediate-mass star close to the main sequence seems to be a key problem for this scenario.

The high-density circumstellar matter and the gaseous ionized disk-like structure speak for rather high mass loss. This mass loss must have been much higher than in the case of classical Be stars, forming disk-like or spiral arm structures, if the material was expelled from some hot spots on the stellar surface and expanding outwards. Because of the much higher initially released masses in equatorial direction, the density in the outer regions will have ideal conditions for the production of the forbidden emission lines. This mass loss might be less than in the case of B[e] stars. Then, in agreement with Jaschek et al. (1993), we might claim that HD 50138 is “a transition object between Be and B[e] stars”.

– Binary system:

For such a star to have a large amount of dust, as seen in its SED, another possible scenario would be linked to a binary component, where the dust could be formed in a long-lived circumbinary disk or by wind collisions. Baines et al. (2006) suggest that the (possible) separation of components would be at least $0.''5$. However, considering the possible distance of HD 50138, this separation would be very large to have mass exchange (250 AU considering the smallest angular separation), which could explain the spectral and photometric variability of this object. This would also hamper the possible classification of this star as FS CMa star (Miroshnichenko 2007), since this group of stars is tentatively classified as objects close to or still on the main sequence in binary systems with mass exchange.

On the other hand, since the radius of the FEROS aperture is $1''$, in principle, there might be a chance that we observed both components at the same time. However, we could not find any spectral feature to confirm the existence of a secondary component. This result also agrees with Corporon & Lagrange (1999), who searched for TTauri companions in a sample of HAeBe candidates, based on several diagnostic lines, e.g. from CaI, FeI and LiI. They did not find any evidence of binarity for HD 50138. However, an HAeBe star as a companion could not be completely discarded. Thus, at this moment we can neither confirm nor exclude a possible binary nature for HD 50138.

– Other classes of B[e] stars:

Since HD 50138 shows the B[e] phenomenon, we should also discuss the possibility that it belongs to one of the other known classes of objects that present it (Lamers et al. 1998). However, based on the absence of typical nebular and symbiotic lines in its spectrum, we can discard a compact planetary nebula and a symbiotic nature for this object. In addition, the low luminosity, in combination with no indication of nitrogen enrichment, exclude a supergiant scenario for this star. However, since almost 50% of the objects with the B[e] phenomenon are considered unclassified, we cannot exclude that HD 50138 might be an object that represents a link between Be and B[e] stars.

5. Conclusions

HD 50138 is a very curious star that displays strong spectroscopic variations. Based on analysis of new high-resolution data, we present a detailed description of these variations. Our analysis of the photometric data suggests that HD 50138 is a B6-7 III-V star, whose luminosity was tentatively obtained from a careful study of the influence of the possible circumstellar extinction sources and based on the new Hipparcos distance. A new value for the color excess, $E(B - V) = 0.08 \pm 0.01$ mag, was derived. In addition, we suggest that a new-shell phase or the formation of one-armed spiral could have taken place before 2007.

Based on our results, a pre-main sequence star or a transition object between Be and B[e] stars, close to or just at the turn-off from the main sequence, or a binary scenario, can be neither confirmed nor discarded; however, an observational campaign, based on photometry, to derive a detailed light-curve and high-resolution spectroscopy associated to a detailed analysis in terms of the line profile appearances and variations have to be performed to confirm the possible shell phases and the slow-down of this star. A careful interferometric analysis, associated to a SED modeling considering different scenarios for the circumstellar dust is in progress (Borges Fernandes et al., in prepara-

tion) and will certainly provide better constraints for the circumstellar geometry and the nature of this curious star.

Acknowledgements. This research made use of the NASA Astrophysics Data System (ADS) and of the SIMBAD, VizieR and 2MASS databases. M.B.F. acknowledges financial support from the Programme National de Physique Stellaire (France) and the Centre National de la Recherche Scientifique (CNRS-France) for the post-doctoral grant. M.K. acknowledges financial support from GA AV ČR number KJB300030701. M.B.F. and F.X.A. acknowledge Dr. Victor de Amorim d'Ávila to perform the observations at ESO (La Silla, Chile). A.D.S. acknowledges Dr. Michel Auriere to perform the observations at the Observatoire Midi Pyrenees (France). M.B.F. acknowledges Dr. Pierre Cruzalébes for his help with Hakkila et al. (1997) software. We acknowledge Dr. Adéla Kawka for comments on the manuscript and we also wish to thank Dr. Jiří Kubát for providing us with his databases computed with SYNSPEC.

References

- Allen, D. A. 1973, *MNRAS*, 161, 145
 Alvarez, M., & Schuster, W. J. 1981, *Rev. Mex. A&A*, 6, 163
 Andriillat, Y., & Houziaux, L. 1972, *Ap&SS*, 18, 324
 Andriillat, Y., & Houziaux, L. 1991, *IAUC*, 5164, 3
 Arenou, F., Grenon, M., & Gomez, A. 1992, *A&A*, 258, 104
 Baines, D., Oudmaijer, R. D., Porter, J. M., & Pozzo, M. 2006, *MNRAS*, 367, 737
 Bernasconi, P. A., & Maeder, A. 1996, *A&A*, 307, 829
 Bjorkman, K. S., Miroshnichenko, A. S., Bjorkman, J. E., et al. 1998, *ApJ*, 509, 904
 Bopp, B. W. 1993, *IBVS*, 3834, 1
 Borges Fernandes, M., Kraus, M., Lorenz Martins, S. & de Araújo, F.X. 2007, *MNRAS*, 377, 1343
 Cardelli, J. A., Clayton, G. C., & Mathis, J. S. 1989, *ApJ*, 345, 245
 Chen, B., Vergely, J. L., Valette, B., & Carraro, G. 1998, *A&A*, 336, 137
 Cidale, L., Zorec, J., & Tringaniello, L. 2001, *A&A*, 368, 160
 Corporon, P., & Lagrange, A.-M. 1999, *A&AS*, 136, 429
 de Winter, D., van den Ancker, M. E., Maira, A., et al. 2001, *A&A*, 380, 609
 Doazan, V. 1965, *AnAp*, 28, 1
 Flower, P. J. 1996, *ApJ*, 469, 355
 Frémat, Y., Neiner, C., Hubert, A.-M., et al. 2006, *A&A*, 451, 1053
 Hakkila, J., Myers, J. M., Stidham, B. J., & Hartmann, D. H. 1997, *AJ*, 114, 2043
 Halbedel, E. M. 1991, *Inf. Bull. Var. Stars*, No. 3585, 1
 Hamann, F. 1994, *ApJSS*, 93, 485
 Harrington, D. M., & Kuhn, J. R. 2007, *ApJ*, 667, 89
 Harrington, D. M., & Kuhn, J. R. 2009, *ApJS*, 180, 138
 Haupt, H. F., & Schroll, A. 1974, *A&AS*, 15, 311
 Herbig, G. H. 1993, *ApJ*, 407, 142
 Houziaux, L. 1960, *JO*, 43, 217
 Houziaux, L., & Andriillat, Y. 1976, in *Be and Shell Stars*, ed. A. Slettebak (Dordrecht: Reidel), IAU Symp. No. 70, 87
 Hubeny, I., & Lanz, T. 2000, *SYNSPEC - A User's Guide*
 Hutsemékers, D. 1985, *A&AS*, 60, 373
 Jaschek, C., & Andriillat, Y. 1998, *A&AS*, 128, 475
 Jaschek, M., Jaschek, C., & Andriillat, Y. 1993, *A&AS*, 97, 781
 Kilkenny, D., Whittet, D. C. B., Davies, J. K., et al. 1985, *South African Astron. Obs. Circ.*, no. 9, 55
 Kraus, M., Kubát, J., & Krtička, J. 2008, *A&A*, 481, 499
 Kraus, M., Borges Fernandes, M., & Kubát, J. 2009, *A&A*, 499, 291
 Kurucz, R. L. 1979, *ApJS*, 40, 1
 Kurucz, R. L. 1993, *Atomic Data for Opacity Calculations*, Kurucz CD-ROM No. 1
 Lamers, H. J. G. L. M., Zickgraf, F.-J., de Winter, D., Houziaux, L., & Zorec, J. 1998, *A&A*, 340, 117
 Landaberry, S.J.C., Pereira, C.B., & de Araújo, F.X. 2001, *A&A*, 376, 917
 Leitherer, C., & Wolf, B. 1984, *A&A*, 132, 151
 Mathis, J.S., 1990, *ARA&A* 28, 37
 Mathis, J. S., Ruml, W., Nordsieck, K. H. 1977, *ApJ*, 217, 425
 Merrill, P. W., Humason, M. L., & Burwell, C. G. 1925, *ApJ*, 61, 389
 Merrill, P. W. 1931, *ApJ*, 73, 348
 Merrill, P. W., & Burwell, C. G. 1933, *ApJ*, 78, 87
 Miroshnichenko, A. S. 2007, *ApJ*, 667, 497
 Moore, C.E. 1945, *A Multiplet Table of Astrophysical Interest, Part I - Table of Multiplets* (Revised Ed., Princeton, New Jersey: Princeton University Observatory)
 Neckel, Th., Klare, G. & Sarcander, M. 1980, *A&AS*, 42, 251
 Oudmaijer, R. D., & Drew, J. E. 1999, *MNRAS*, 305, 166
 Penston, M. J. 1973, *MNRAS*, 164, 133

- Perryman, M. A. C., & ESA 1997, The Hipparcos and Tycho Catalogues, ESA SP Series vol. 1200 (Nordwijk: ESA)
- Pogodin, M. A. 1997, A&A, 317, 185
- Schaller, G., Schaerer, D., Meynet, G., & Maeder, A. 1992, A&AS, 96, 269
- Schmidt-Kaler, Th. 1982, in Landolt-Börnstein, New Series, Group IV, Vol. 2b, (eds.) K. Schaifers & H. H. Voigt, Springer, Berlin, 1
- Stee, Ph., & Bittar, J. 2001, A&A, 367, 532
- Thackeray, A. D. 1967, MNRAS, 135, 51
- Vaidya, A., Schulte-Ladbeck, R. E., & Bjorkman, K. S. 1994, AAS, 184, 4411
- van Leeuwen, F. 2007, A&A, 474, 653
- Waters, L. B. F. M., & Waelkens, C. 1998, ARA&A, 36, 233
- Zorec, J., & Briot, D. 1991, A&A, 245, 150
- Zorec J. 1998, in B[e] Stars, Astrophysics and Space Science Library, ed. Hubert, A. M. and Jaschek, C., 27

Table 1. Lines identified in our FEROS spectra obtained in 1999 and 2007. The observed central wavelength (λ_{obs}), radial velocity (v_{rad}), equivalent width of emission (W_{em}) and/or absorption (W_{abs}) components and identification of the lines seen in each date are provided.

1999					2007					Identification
λ_{obs}	v_{rad}	W_{em}^{blue}	W_{abs}	W_{em}^{red}	λ_{obs}	v_{rad}	W_{em}^{blue}	W_{abs}	W_{em}^{red}	
					3704.3	32.4		0.79		H16 3703.9
					3712.4	32.3		1.07		H15 3712.0
					3722.5	48.4		1.48		H14 3721.9
					3735.0	48.2		2.46		H13 3734.4
					3750.9	56.0		3.37		H12 3750.2
					3771.4	63.7		4.87		H11 3770.6
					3798.6	55.3		5.45		H10 3797.9
					3820.4	47.1		0.22		He I (m22) 3819.8
										He I (m22) 3819.6
					3835.9	39.1		5.81		H9 3835.4
					3850.0			0.04		Uid
					3854.0	23.4		0.05		Si II (m1) 3853.7
					3856.5	38.9		0.19		Si II (m1) 3856.0
					3863.1	38.8		0.15		Si II (m1) 3862.6
					3868.0	38.8		0.04		He I (m20) 3867.6
					3889.6	46.3		6.32		H8 3889.1
										He I (m2) 3888.7
3970.3	15.1		6.93		3934.1	30.5	0.11	0.80	0.07	Ca II (m1) 3933.7
					3970.7	45.3		7.84		He I 3970.1
										Ca II (m1) 3968.5
					4003.0	30.0		0.02		Fe II (m190) 4002.6
					4009.6	22.5		0.07		He I (m55) 4009.3
4026.8	44.7		0.41		4026.5	22.4		0.36		He I (m18) 4026.2
4102.1	29.3		5.93		4102.5	58.5		6.82		H δ 4101.7
4121.6	43.7		0.06		4121.5	36.4		0.02		He I (m16) 4121.0
4128.8	47.4		0.17		4128.6	36.3		0.13		Si II (m3) 4128.1
4131.6	47.2		0.24		4131.4	36.3		0.14		Si II (m3) 4130.9
4144.8	72.4		0.18		4144.6	57.9		0.14		He I (m53) 4143.8
					4164.1			0.02		Uid
4173.6	7.2		0.06		4174.1	43.1		0.08		Fe II (m27) 4173.5
4178.9	0.0		0.08		4179.4	36.0		0.12		Fe II (m28) 4178.9
										Fe II (m21) 4177.7
4233.7	35.4	0.06	0.09	0.11	4233.6	28.4	0.13	0.16	0.13	Fe II (m27) 4233.2
4244.5	35.3			0.04						[Fe II] (m21F) 4244.0
					4258.8	42.3		0.01		Fe II (m28) 4258.2
					4262.6	49.3		0.02		Cr II (m31) 4261.9
										Cr II (m17) 4261.8
4268.0	70.3		0.04		4267.8	56.3		0.05		C II (m6) 4267.0
										C II (m6) 4267.2
										C II (m6) 4267.3
					4273.9			0.01		Uid
4277.3	35.1			0.03	4277.3	35.1			0.03	[Fe II] (m21F) 4276.8
4287.9	35.0			0.04	4287.9	35.0			0.08	[Fe II] (m7F) 4287.4
4290.3	7.0		0.02		4290.9	49.0		0.04		Ti II (m41) 4290.2
4294.2	7.0		0.02		4294.7	41.9		0.04		Ti II (m20) 4294.1
					4297.1	34.9		0.06		Fe II (m28) 4296.6
4300.5	27.9	0.06	0.02	0.10	4300.5	27.9		0.07		Ti II (m41) 4300.1
					4303.8	41.8		0.04		Fe II (m27) 4303.2
					4320.0				0.02	Uid
4340.6	6.9		4.30		4340.9	27.7		5.31		Hy 4340.5
4352.4	41.4		0.07	0.07	4352.2	27.6	0.08	0.07	0.08	Fe II (m27) 4351.8
4359.6	20.7			0.09	4359.7	27.5			0.10	[Fe II] (m7F) 4359.3
										[Fe II] (m21F) 4358.4
					4369.3			0.06		Uid
4385.4	54.7		0.06		4385.9	34.2		0.13		Mg II 4384.6
4388.6	47.9		0.15		4388.6	47.7		0.21		He I (m51) 4387.9
4391.4	54.7		0.07		4391.2	41.0		0.13		Mg II (m10) 4390.6
										Fe II (m27) 4389.9
4395.6	41.0		0.04	0.04	4395.5	34.1	0.10	0.02	0.08	Ti II (m19) 4395.0

Table 1. Continued.

1999					2007					Identification
λ_{obs}	v_{rad}	W_{em}^{blue}	W_{abs}	W_{em}^{red}	λ_{obs}	v_{rad}	W_{em}^{blue}	W_{abs}	W_{em}^{red}	
4444.5	47.3		0.02	0.04	4443.6	-13.5	0.07	0.01	0.03	Ti II (m19) 4443.8
					4458.4	26.9			0.03	[Fe II] (m6F) 4458.0
4472.4	47.0		0.34		4472.2	33.5		0.29		He I (m14) 4471.7
4482.2	60.3		0.47		4482.0	43.4		0.36		Mg II (m4) 4481.3
					4489.8	40.1		0.02		Fe II (m37) 4489.2
					4492.1	46.8		0.01		Fe II (m37) 4491.4
4502.1	55.3		0.1	0.04	4501.1	-11.3	0.07	0.01	0.03	Ti II (m31) 4501.3
4508.7	26.6		0.04	0.02	4508.6	20.0	0.06	0.07	0.04	Fe II (m38) 4508.3
4515.8	39.9		0.03	0.01	4516.0	46.5		0.05		Fe II (m37) 4515.3
										Fe II (m20) 4515.2
4520.8	39.8		0.02	0.02	4520.8	39.8		0.01		Fe II (m37) 4520.2
4523.2	39.8		0.06	0.05	4523.3	46.4	0.04	0.10	0.06	Fe II (m38) 4522.6
4534.5	35.1		0.03	0.04	4533.9	-4.7	0.07	0.02	0.04	Ti II (m50) 4534.0
										Fe II (m37) 4534.2
					4542.2	46.2		0.01		Fe II (m38) 4541.5
4550.0	33.0		0.13	0.11	4549.9	26.4	0.14	0.16	0.12	Fe II (m38) 4549.5
4556.6	46.1		0.04	0.04	4556.6	46.1	0.02	0.06	0.04	Fe II (m37) 4555.9
4558.9	26.3		0.05	0.02	4559.4	52.7		0.09		Fe II (m20) 4558.6
4564.2	26.3		0.01	0.02	4564.4	39.4		0.03		Ti II (m50) 4563.8
4572.5	32.8		0.03	0.04	4572.5	32.8	0.09	0.01	0.07	Ti II (m82) 4572.0
					4576.8	32.8		0.06		Fe II (m38) 4576.3
4584.5	45.8		0.11	0.13	4584.4	39.3	0.20	0.12	0.23	Fe II (m38) 4583.8
										Fe II (m26) 4584.0
4588.3	6.5		0.05		4588.9	45.8		0.06		Cr II (m44) 4588.2
										Cr II (m16) 4588.4
					4592.7	39.2		0.02		Cr II (m44) 4592.1
					4596.6	58.8		0.04		Fe II (m38) 4595.7
					4619.5	45.5		0.03		Cr II (m16) 4618.8
										C II 4618.9
4630.2	58.3		0.01	0.05	4630.1	51.8	0.07	0.04	0.07	Fe II (m37) 4629.3
					4635.5	58.3		0.07		Fe II (m25) 4634.6
					4640.1				0.01	Uid
4713.9	31.8		0.08		4713.8	25.5		0.06		He I (m12) 4713.4
					4732.2	50.7		0.02		Fe II (m43) 4731.4
4814.9	18.7			0.05	4814.9	18.7			0.05	[Fe II] (m20F) 4814.6
4824.4	18.7		0.03		4824.9	24.9	0.03	0.04	0.01	Cr II (m30) 4824.1
										S II (m52) 4824.1
4848.5	18.6			0.03	4849.0	49.5		0.04		Cr II (m30) 4848.2
										Fe II (m30) 4847.6
4862.8	92.6		0.26		4862.8	92.6		0.21		H β 4861.3 ²
4876.7	18.5		0.02		4877.1	43.1		0.03		Cr II (m30) 4876.4
										Cr II (m30) 4876.5
4890.3	43.0			0.04	4890.1	30.7			0.03	[Fe II] (m4F) 4889.6
										[Fe II] (m3F) 4889.7
					4905.9	30.6			0.02	[Fe II] (m20F) 4905.4
4924.8	54.8		0.26	0.40	4925.0	67.0	0.20	0.29	0.35	Fe II (m42) 4923.9
5019.5	65.8	0.03	0.28	0.57	5019.4	59.8	0.31	0.34	0.48	Fe II (m42) 5018.4
5041.9	47.6		0.11		5041.7	35.7		0.08		Si II (m5) 5041.1
5048.4	41.6		0.06		5048.4	41.6		0.03		He I (m47) 5047.7
5057.2	47.5		0.20		5056.7	17.8		0.12		Si II (m5) 5056.4
					5094.1			0.01		Uid
					5101.6	35.3		0.03		Fe II 5101.0
5159.3	75.6			0.10	5159.1	64.0			0.13	[Fe II] (m18F) 5158.0
5169.7	40.6	0.13	0.42	0.48	5170.0	58.0	0.30	0.50	0.45	Fe II (m42) 5169.0
5198.7	63.5		0.04	0.07	5198.3	40.4	0.10	0.05	0.11	Fe II (m49) 5197.6
					5228.0			0.03		Uid
5235.6	57.3		0.05	0.09	5235.2	34.4	0.09	0.06	0.06	Fe II (m49) 5234.6

² Because of the complexity of the profile, the equivalent width of H β (and also of H γ and H δ) was derived considering the total one, i.e., the equivalent width of the absorption component minus that one from the emission components.

Table 1. Continued.

1999					2007					Identification
λ_{obs}	v_{rad}	W_{em}^{blue}	W_{abs}	W_{em}^{red}	λ_{obs}	v_{rad}	W_{em}^{blue}	W_{abs}	W_{em}^{red}	
5262.4	45.6			0.08	5262.3	39.9			0.06	[Fe II] (m19F) 5261.6
5276.6	34.1	0.07	0.03	0.12	5276.2	11.4	0.14	0.20	0.10	Fe II (m49) 5276.0
					5284.3	11.4	0.03	0.01	0.02	Fe II (m41) 5284.1
5317.8	67.7	0.06	0.02	0.30	5317.3	39.5	0.23	0.09	0.21	Fe II (m49) 5316.6
					5334.1	22.5			0.06	[Fe II] (m19F) 5333.7
5364.2	72.7			0.06	5363.1	56.0	0.06	0.03	0.05	[Fe II] (m17F) 5362.1
5377.0	27.9			0.02	5377.0	27.9			0.03	[Fe II] (m19F) 5376.5
					5467.7			0.04		Uid
					5528.0	38.0			0.03	[Fe II] (m17F) 5527.3
										[Fe II] (m34F) 5527.6
					5535.5	32.5	0.05	0.01	0.05	Fe II (m55) 5534.9
5577.9	32.3			0.04	5578.1	43.0			0.03	[O I] (m3) 5577.3
5876.8	61.3	0.13	0.53		5876.1	25.5	0.08	0.23	0.05	He I (m11) 5875.6
5890.4	20.4		0.73	0.19	5890.6	30.6		0.59		Na I (m1) 5890.0
5896.5	30.5		0.49	0.14	5896.6	35.6		0.39		Na I (m1) 5895.9
					6149.3	4.9		0.08		Fe II (m74) 6149.2
6158.4	9.7		0.14		6158.2	68.2		0.12		O I (m10) 6158.2
										O I (m10) 6156.8
					6176.1	45.7		0.03		Fe II (m200) 6175.2
6238.6	9.6		0.03		6239.4	48.1		0.08		Fe II (m74) 6238.4
6248.6	48.0		0.05	0.06	6248.7	52.8	0.03	0.05	0.06	Fe II (m74) 6247.6
6301.1	38.1			0.55	6301.1	38.1			0.58	[O I] (m1F) 6300.3
6319.0	38.0			0.12	6318.9	33.2			0.19	Mg I (m23) 6318.2
										Mg I (m23) 6318.8
										Fe II 6318.0
6348.6	70.9		0.54		6347.5	18.9	0.05	0.32		Si II (m2) 6347.1
6364.6	37.7			0.20	6364.6	37.7			0.21	[O I] (m1F) 6363.8
6372.9	70.6		0.35		6371.7	14.1	0.04	0.22		Si II (m2) 6371.4
6385.6	86.9			0.11	6385.1	63.5			0.18	Fe II 6383.8
										Fe II (m203) 6387.6
					6417.8	42.1		0.04		Fe II (m74) 6416.9
6457.7	60.4		0.06	0.06	6457.1	51.1	0.10	0.07	0.10	Fe II (m74) 6456.4
6564.8	91.4			61.35	6564.1	59.4			57.56	H α 6562.8
6680.1	85.4		0.34		6678.7	22.5	0.03	0.12	0.03	He I (m46) 6678.2
7067.0	76.4		0.10		7066.1	38.2	0.02	0.06	0.04	He I (m10) 7065.2
										He I (m10) 7065.7
7496.5				0.13	7497.1				0.15	Uid
7515.0				0.31	7514.2				0.36	Uid
7713.0	50.6			0.26	7712.2	54.5	0.11	0.01	0.06	Fe II (m73) 7711.7
7773.5	57.9	0.20	1.61		7774.4	92.6	0.25	1.77	0.41	O I (m1) 7772.0
										O I (m1) 7774.2
										O I (m1) 7775.4
8325.3				0.20						Uid
8346.9	32.4			0.31						H I P23 8346.0
8360.0	35.9			0.31						H I P22 8359.0
8375.5	35.8			0.61	8374.8	10.8			0.86	H I P21 8374.5
8393.5	39.3			0.80	8392.4	0.0			1.07	H I P20 8392.4
8414.2	32.1			0.75	8413.7	14.3			1.33	H I P19 8413.3
8440.0				0.76	8435.8				0.85	Uid
8448.1	46.2			4.01	8447.1	10.7			3.70	O I (m4) 8446.8
8468.8	53.2			1.08	8468.6	46.1			1.40	H I P17 8467.3
8501.4	-38.8			2.35	8500.9	0.0			2.29	H I P16 8502.5
										Ca II (m2) 8498.0
8598.8	14.0			1.85	8598.2	-7.0			1.86	H I P14 8598.4
8630.7	52.2			1.14	8630.6	48.7			1.73	N I (m8) 8629.2
8664.9	-3.5			2.79	8664.3	-24.2			2.94	H I P13 8665.0
										Ca II (m2) 8662.1
8684.0	20.7			0.47						N I (m1) 8683.4
8751.8	44.6			2.24	8751.9	48.0			2.27	H I P12 8750.5